Laser Chem. 1983, Vol. 2, pp. 137–166
0278–6273/83/0206–0137$12.00/0

Printed in Great Britain

Very Low Energy Collision Induced Vibrational Relaxation: An Overview

STUART A. RICE and CHARLES CERJAN

The Department of Chemistry and the James Franck Institute, The University of Chicago, Chicago, Illinois 60637

Recent experimental and theoretical studies of very low energy collision induced vibrational relaxation in diatomic and polyatomic molecules are surveyed. Emphasis is placed on the novel features of the very low energy process; these require a full quantum mechanical treatment of the collision to account for the observations.

1. INTRODUCTION

Although collision induced vibrational relaxation has been studied for many years, it has only recently been discovered that very low energy collisions can lead to very efficient energy transfer.[1] Conventional theories, such as that due to Schwartz, Slawsky and Herzfeld,[2] predict that the vibrational relaxation cross section decreases as the collision energy decreases, and is vanishingly small for collision energies near 1 cm^{-1}. This prediction is in complete disagreement with experiments in a variety of systems, all of which imply that the very low energy vibrational relaxation cross section is of the order of magnitude of the (geometric) collision cross section.[3–6]

This paper presents an overview of the extant experiments[3–8] and theoretical[9,10] studies of very low energy collision induced relaxation phenomena. We shall show that both qualitative and quantitative interpretations of the observed behavior follow from a full quantum mechanical treatment of the atom–molecule collision.

2. EXPERIMENTAL METHOD

The most direct way of studying atom–molecule collision induced vibrational relaxation employs crossed, velocity selected, molecular beams. The conditions employed to generate molecular beams make it difficult to study the very low collision energy regime; to date only one such study has been reported.[11] The overwhelming majority of atom–molecule collision induced vibrational relaxation studies, irrespective of the collision energy range of interest, are carried out under "bulb conditions." In these experiments the average collision energy is varied by changing the temperature; and the lowest temperature that can be achieved is limited by a thermodynamic constraint, namely, condensation of one or both of the species that define the collision.

Rice and co-workers have devised a method for bypassing the thermodynamic constraint characteristic of bulb studies, thereby permitting study of the collision energy dependence of vibrational relaxation in the very low collision energy regime.[3] Their method takes advantage of the characteristics of supersonic free jets. In a supersonic

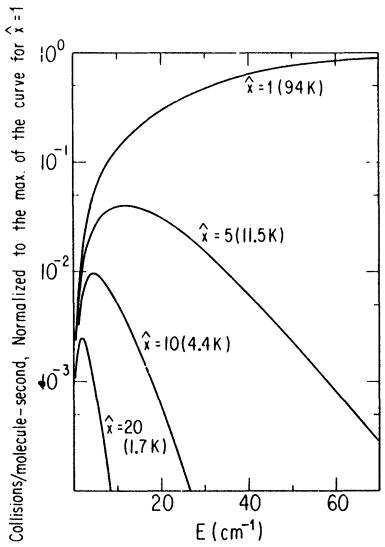

FIGURE 1 Number of collisions per molecule per second in a free jet as a function of distance from the nozzle, measured in nozzle diameters.

jet, generated by adiabatic expansion through a nozzle, the translational temperature and density of the gas varies with distance from the nozzle. The residual collisions characteristic of the temperature at any given distance from the nozzle can be used to induce vibrational relaxation in an excited seeded molecular species. Thus, by changing the downstream location of the excitation region and dispersing the fluorescence it is possible to probe the effect of collision energy on vibrational relaxation. Calculations based on the kinetic theory of the jet show that the collision energy range that can be studied is of the order $100-1\ \mathrm{cm}^{-1}$ for a gas originally at 300 K, and it can be extended upwards by heating the nozzle. Furthermore, the range of collision energies selected is very narrow when the local temperature is low (Figure 1). Finally, by adjusting the carrier gas pressure it can be arranged that there are one or less collisions per lifetime, or if so desired that there are several collisions per lifetime, of the excited molecule with carrier gas molecules.

A few details concerning the properties of free supersonic jets are pertinent to our discussion. Under reversible adiabatic flow conditions the supersonic expansion is isentropic and, for an ideal gas,[12]

$$\frac{T}{T_0}=\left(\frac{n}{n_0}\right)^{\gamma-1} \tag{1}$$

where n is the gas density, $\gamma = C_p/C_v$, the ratio of heat capacities, and the subscript zero refers to conditions in the source. If the expansion is considered to originate from a source sphere of radius r_*, the temperature of the gas along the jet centerline is, for Mach number $M \gg 1$,

$$\frac{T}{T_0}=\frac{2}{\gamma+1}\left(\frac{\gamma-1}{\gamma+1}\right)^{(\gamma-1)/2}\left(\frac{x}{r_*}\right)^{-2(\gamma-1)} \tag{2}$$

where x is the axial distance downstream and r_* depends on the nozzle diameter D.[13]

Sufficiently far downstream the gas density decreases to the point that the assumption of hydrodynamic flow, made above, ceases to be valid, and the velocity distribution for motion parallel to the jet is characterized by a different temperature ($T_\parallel$) than that for motion perpendicular to the jet ($T_\perp$). Cattolica, Robben, Talbot and Willis[13] have shown, from an extensive investigation of the domain of validity

of hydrodynamic flow in free jets, that as p_0D increases the ellipsoidal velocity distribution becomes nearly spherical (p_0 is the source pressure). Rice and coworkers choose source conditions such that the difference between $T_\parallel$ and $T_\perp$ is small for all x used in the experiment, so that the velocity distribution function at any position x can be characterized by one temperature, T. Cattolica *et al.* have shown that $(r_*/D) = 0.742$ in this p_0D regime.

Consider some point x along the jet axis, at which the local temperature is $T(x)$. The differential number of collisions per seeded molecule per unit time is

$$dZ = \pi\sigma^2 |\mathbf{v}_r| f_1(\mathbf{v}_1) f_2(\mathbf{v}_2)\, d\mathbf{v}_2 \tag{3}$$

with

$$f_i(\mathbf{v}_i) = \left(\frac{m_i}{2\pi k_B T}\right)^{3/2} \exp\left\{-\frac{m_i}{2k_B T}[(v_{xi}-u)^2 + v_{yi}^2 + v_{zi}^2]\right\} \tag{4}$$

The carrier gas is labelled 1, the seed species is labelled 2, $\pi\sigma^2$ is the seeded molecule-carrier gas molecule collision cross section (assumed constant), $\mathbf{v}_r$ is the relative velocity between carrier gas and seeded species molecules, and $\mathbf{u}$ is the bulk flow velocity. After transformation to center-of-mass and relative coordinates, and integration, the total number of collisions per seeded molecule per unit time with relative speed between v_a and v_b is found to be

$$Z^{ab} = \left(\frac{2}{\pi}\right)^{1/2} n_1 \pi\sigma^2 \left(\frac{\mu}{k_B T}\right)^{3/2} \int_{v_a}^{v_b} dv_r\, v_r^3\, e^{-\mu v_r^2/2k_B T} \tag{5}$$

where μ is the reduced mass of the colliding pair. Given the functional forms for $n(x)$ and $T(x)$ implicit in Eqs. (1) and (2), Eq. (5) is conveniently rewritten in the form

$$Z^{ab} = C\pi\sigma^2 \hat{x}^{-8/3} [e^{-y}(y+1)]_{y_b}^{y_a} \tag{6}$$

where we have assumed the carrier gas is monoatomic with $\gamma = 5/3$. In (6), C is a constant, $\hat{x} = x/D$ and

$$y = 1.58\left(\frac{\mu v^2}{k_B T_0}\right)\hat{x}^{4/3} \tag{7}$$

Values of Z^{ab} for representative collision parameters and source conditions are displayed in Table I.

TABLE I.
Collisions/molecule-s for $p_0 = 30$ psi; He carrier gas, $T_0 = 300\,K$

Integration range (cm^{-1})	$\hat{x} = 4$	$\hat{x} = 20$
(0, 1)	5.87×10^5	3.68×10^5
(0, 5)	1.14×10^7	1.68×10^6
(0, 10)	3.38×10^7	1.83×10^6
(0, 100)	1.34×10^8	1.83×10^6
(0, ∞)	1.34×10^8	1.83×10^6

3. A SURVEY OF EXPERIMENTAL FINDINGS AND QUALITATIVE INTERPRETATIONS

The available data base concerning very low energy collision induced vibrational relaxation consists of studies involving $I_2(^3\Pi_{o_u^+})$, $C_6H_5NH_2(^1B_2)$, $C_6H_5CH_3(^1B_2)$, $C_6H_5F(^1B_2)$, $C_6H_6(^1B_{2u})$ and $C_2H_2O_2(^1A_u)$. We shall cite particular points from the results of each of these studies.

In the experiments by Tusa, Sulkes and Rice, I_2 was seeded in He, Ne or Ar, a particular vibrational level of $I_2(^3\Pi_{o_u^+})$ was excited, and the vibrational relaxation to other levels followed as a function of relative kinetic energy of the collision partners.[1,3] Typical results for I_2 in He are shown in Figures 2, 3 and 4. The conditions employed

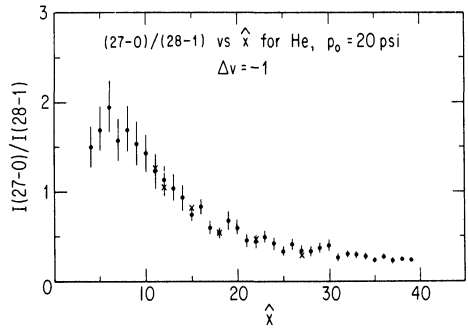

FIGURE 2 Relative intensity of levels 27 and 28 of $I_2(^3\Pi_{o_u^+})$ as a function of distance from the nozzle. The system was initially excited to level 28. The crosses represent the calculated ratio of intensities under the assumption that all collisions with $0 \leq E \leq 3\ cm^{-1}$ are equally effective. Collision partner: He.

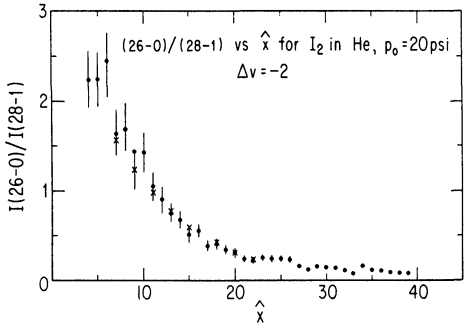

FIGURE 3 Same as Figure 2 except for monitoring of level 26.

in obtaining the data of Figure 2 correspond to their being one He : I_2 collision per excited state lifetime, whereas there were, respectively, two and three collisions per lifetime for the data of Figures 3 and 4. Results for I_2 in Ne, shown in Figures 5, 6, and 7, are similar in the dependence of depopulation of the initial level on relative kinetic energy.

There are two features of these observations that are striking. First, collisional depopulation persists even when the relative kinetic energy of the collision partners is sensibly zero, as shown by the existence of emission from new levels even under conditions where $T \sim 1$ K. Second, the cross section for this proccess is very large. The validity of this point will be demonstrated below.

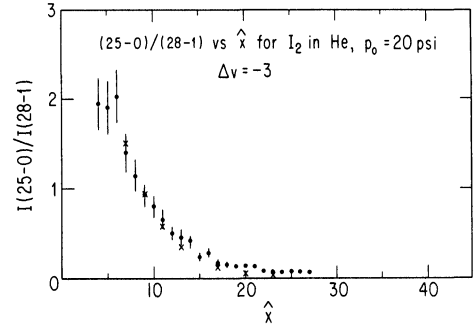

FIGURE 4 Same as Figure 2 except for monitoring of level 25.

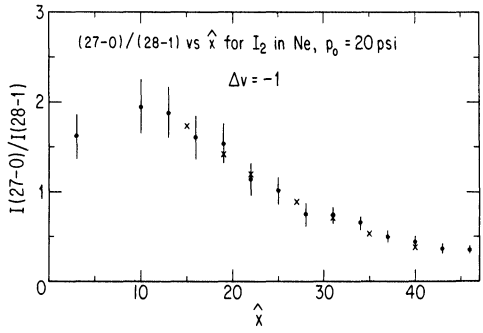

FIGURE 5 Relative intensity of levels 27 and 28 of $I_2(^3\Pi_{o_u^+})$ as a function of distance from nozzle. The system was initially excited to level 28. The crosses represent the calculated ratio of intensities under the assumption that all collisions with $0 \leqslant E \leqslant 1.9\ \text{cm}^{-1}$ are equally effective. Collision partner: Ne.

A consistent interpretation of the observations can be constructed as follows. Suppose collisions wtih $E_{\min} \leqslant E \leqslant E_{\max}$ are equally effective in producing depopulation of the initial vibrational level, and consider the case that there is only one collision per excited state lifetime. The collision energy distribution per molecule-second obtained from the kinetic theory of the jet can be integrated over this range of E for each position along the jet axis. For the correct range ($E_{\min}$, $E_{\max}$) the computed ratio of populations as a function of distance from the nozzle should reproduce the experimental curve. If there is more than one collision per excited state lifetime similar

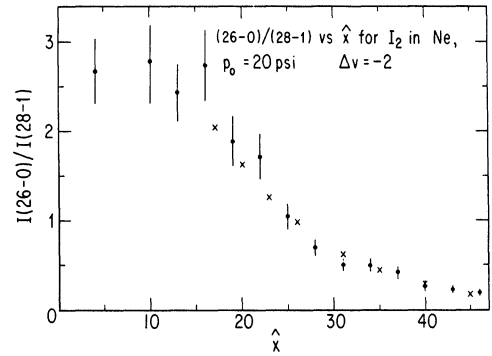

FIGURE 6 Same as Figure 5 except for monitoring of level 26.

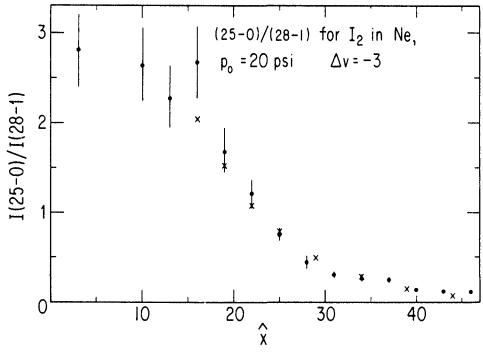

FIGURE 7 Same as Figure 5 except for monitoring of level 25.

calculations can be performed. Tusa, Sulkes and Rice have examined the case of successive collisions, each inducing a one quantum transition, and the case of a single collision inducing two, three, . . . quantum transitions.[3] They find that the experimental data for relaxation of I_2 by He or Ne are well represented by the successive collision-single quantum transfer relaxation model (see Figures 2–7), whereas for relaxation of I_2 by Ar roughly half the population corresponding to $\Delta v = -2$ is generated by a collision which induces a two quantum transition and the other half from succesive collisions that induce single quantum transitions. The energy ranges over which these collisions are effective, computed from the kinetic theory fits to the population decays as a function of position along the jet axis, and assuming a constant cross section equal to the hard sphere collision cross section for the range $E_{\min} \leq E \leq E_{\max}$ and zero for all other E, are displayed in Table II.

Since a successful fit of the kinetic theory-hard sphere collision/relaxation cross section model to their data requires that only very low energy collisions are effective, Sulkes, Tusa and Rice suggest that orbiting resonances, or metastable collision complexes, participate in the relaxation process observed. They also note that the particular collision induced downward transitions monitored in the relaxation of $I_2(^3\Pi_{o_u^+})$ behave similarly when involved in the predissociation of the corresponding van der Waals complex. For example, predissociation of excited HeI_2 and NeI_2 complexes produce $I_2(^3\Pi_{o_u^+})$ with $\Delta v = -1$, whereas for ArI_2 complexes Δv ranges up to -3.

TABLE II
Collisional energy fits for I_2^*—M

Line excited	Gas	p_0 (psi)	T_0 (K)	$\Delta V = -1$	$\Delta V = -2$[a]	$\Delta V = -3$[a]	$\Delta V = -4$[a]
28-0	He	35	297	0–2.4	0–5.5 (1) 0–2.1 (2)	0–11.5 (1) 0–3.1 (2) 0–1.9 (3)	
28–0	He	35	297	0–2.7	0–5.3 (1) 0–1.9 (2)	0–11.4 (1) 0–2.9 (2) 0–1.9 (3)	
16–0	He	31	297	0–2.8	0–6.0 (1) 0–2.9 (2)		
28–0	Ne	35	297	0–1.6	0–4.7 (1) 0–1.3 (2)	0–7.3 (1) 0–1.7 (2) 0–1.0 (3)	
28–0	Ne	31	297	0–1.7	0–5.4 (1) 0–1.6 (2)	0–∞ (1) 0–2.5 (2) 0–1.5 (3)	
28–0[b]	Ne	31	297	0–1.2			
28–0	Ar	35	400	0–2.9	0–3.6 (1) 0–1.5 (2)	0–3.8 (1) 0–1.7 (2) 0–1.1 (3)	
28–0	Ar	31	453	0–2.4	0–3.4 (1) 0–1.5 (2)	0–3.5 (1) 0–1.6 (2) 0–1.0 (3)	0–4.9 (1) 0–2.1 (2) 0–1.3 (3) 0–1.0 (4)

Clearly, the observed very efficient-very low energy collision induced vibrational depopulation of I_2 implies the existence of a relaxation mechanism which is qualitatively different from that dominant at higher collision energy. A simple picture of what that mechanism might be was proposed by Rice and co-workers;[3] a quantitative verification[9] of this picture will be described in Section 4. Briefly, Rice and coworkers observed that at the midpoints of the energy ranges in which the collisions are effective, the de Broglie wavelengths of He, Ne and Ar are 11, 7 and 4 Å, respectively. Therefore, the atom must be treated as having a delocalized wavefunction with spatial extent comparable to or greater than the internuclear spacing of I_2. In general, a vibrational relaxation process is efficient if there are Fourier components of the driving force which are close

to the frequency of the driven oscillator. In an orbiting resonance, or even an "ordinary collision" under the conditions considered herein, the I_2 is effectively embedded in the delocalized wavefunction of the atom, which spreads over the entire molecule. Then, because of the strong repulsion between the I atom and the He atom at small separations, vibration of the I_2 generates amplitude oscillations in the delocalized He spatial distribution, and these in turn create a reaction force at the driving frequency; this reaction force is appropriate for promoting vibrational transitions.

Sulkes, Tusa and Rice also find that there is little or no angular momentum transfer for $\Delta v = 0$ and that for $\Delta v = -1$ the angular momentum transfer occurs predominantly in the range $-6 \leqslant \Delta J \leqslant 6$ ($He : I_2(^3\Pi_{0_u^+})$ system). Blazy *et al.*[14] reached similar conclusions for the rotational state distributions of the $\Delta v = 0$ and $\Delta v = -1$ components of the products following predissociation of the excited $He—I_2$ van der Waals complex. These observations are consistent with the simple mechanism described above if the scattering resonance involves rotational excitation of the I_2 molecule or, in the absence of such excitation, by virtue of the anisotropy of the $He—I_2$ interaction; a more detailed analysis is described in Section 4.

Is it generally the case that very low energy atom–molecule collisions lead to very efficient vibrational relaxation? A partial answer to this question can be obtained from a series of studies by Rice and coworkers.[4,5,6] Briefly put, in all cases studied to date except one, it is observed that:

1) very low energy atom-molecule collisions do lead to efficient vibrational relaxation;

2) the energy ranges in which collisions are efficient are different for vibrations with different point group symmetries;

3) there is a similarity between the relaxation pathways accompanying predissociation of a van der Waals molecule and the corresponding very low energy collision.

An illustration of observation (1) is displayed in Figures 8 and 9, for the case of collisions of He with $^1B_2$ aniline. The spectra show clear evidence for collision induced vibrational relaxation under conditions for which the collision energy is very small. Similar observations have been made for collisions of He with $^1B_2$ toluene, $^1B_2$

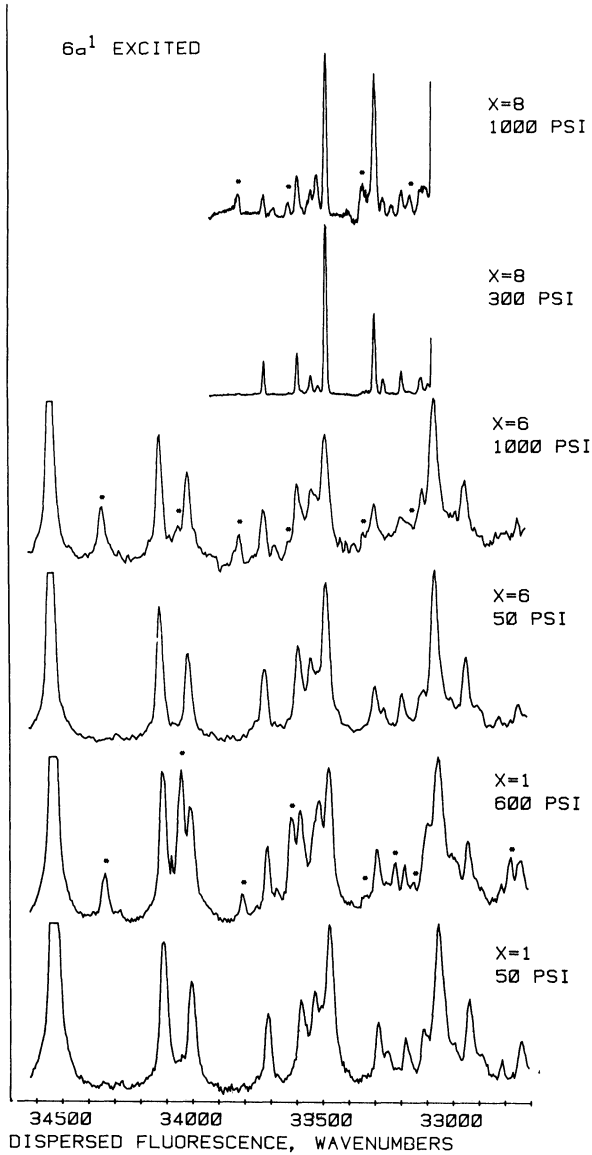

FIGURE 8 Dispersed spectra after $6a^1$ of $^1B_2$ aniline is excited, at successively greater displacements downstream. For each position $\hat{x}$ a low and high p_0 spectrum is shown. Growth bands are denoted with asterisks.

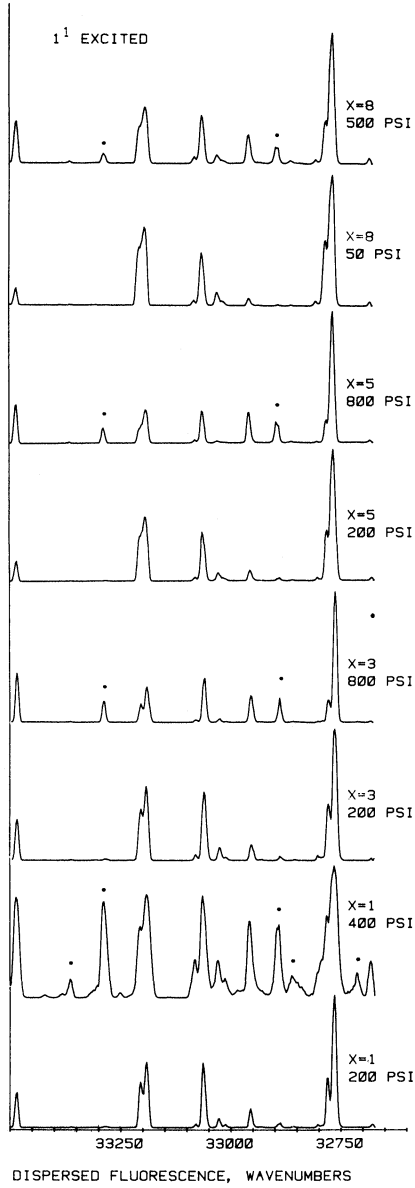

FIGURE 9 Same as Figure 8 except l^1 excited.

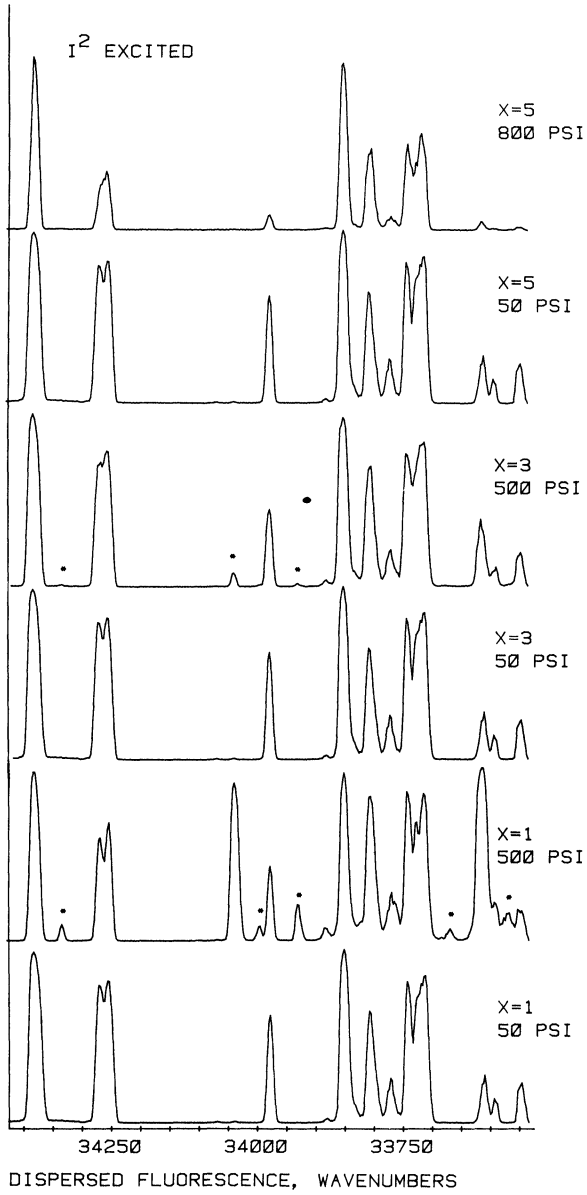

FIGURE 10 Same as Figure 8 except I^2 excited.

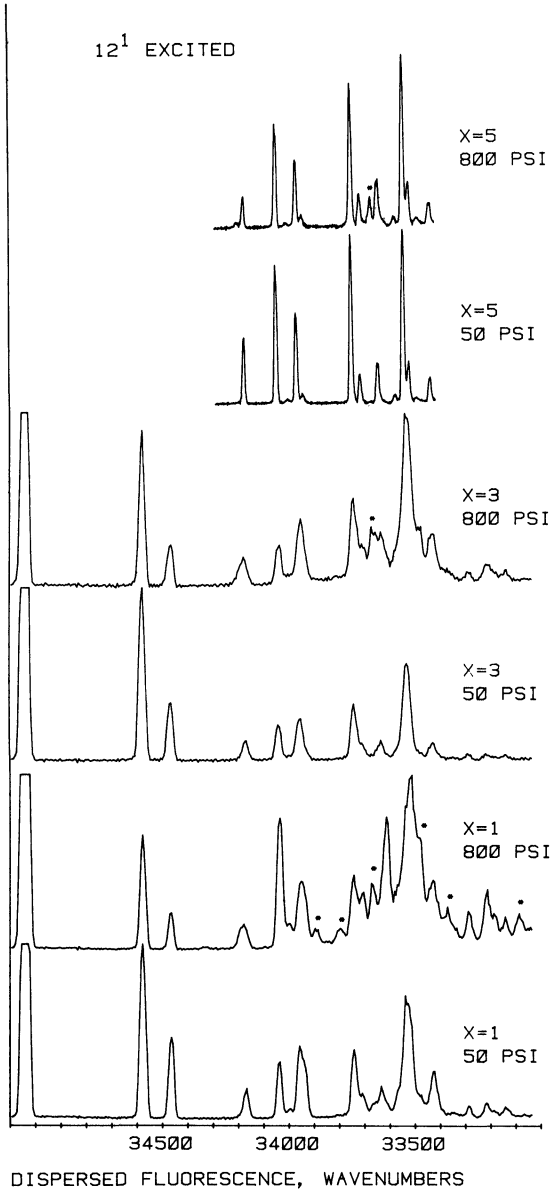

FIGURE 11 Same as Figure 8 except 12^1 excited.

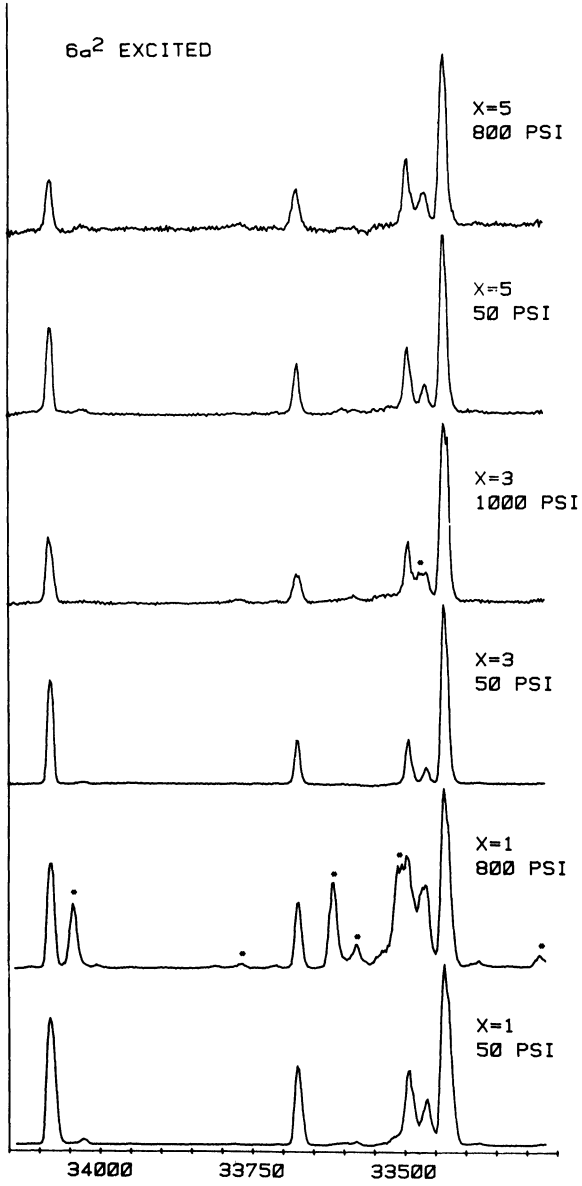

FIGURE 12 Same as Figure 8 except $6a^2$ excited.

fluorobenzene and ^1A_u glyoxal. Different behavior is observed in collisions of He with $^1B_{2u}$ benzene; this observation will be discussed later in this paper.

An illustration of observation (2) can be obtained by comparing Figures 8 and 9 with Figures 10, 11 and 12. It is easily seen that the distance downstream at which collision induced vibrational relaxation ceases is different for vibrations with different point group symmetries.[4] This effect is unambiguous, and has been observed in the very low energy collision regime both for benzene derivatives and for glyoxal. There is no apparent correlation between the energy of effective collisions, which can be deduced from the distance downstream where relaxation ceases, and the energy of the initially pumped vibration. On the other hand, there is a rough correlation between the energy of effective collisions and the number of nodes of the initially pumped vibrational wave function.

An illustration of observation (3) is presented by the entries in Table III. These data show that cold collisions are nearly as selective in generating product states as is van der Waals complex dissociation. It might have been expected (in the sudden approximation to the collision process) that more relaxation pathways would be open in collision induced relaxation than in complex dissociation, corresponding to the many different orientations of collision partners as compared to the well-defined geometry of the complex. It is also noteworthy that three quantum relaxation with a large energy gap ($\sim$1200 cm^{-1})

TABLE III
Growth bands observed

	^1A_u Glyoxal		
Level excited	A Dissociation of H_2 complex	B Low T H_2 coll	C Low T He coll
7^2	$7^1, 0$	$7^1, 0$	$7^1, 0$
5^1	$7^1, 0$	0	0
8^1	0	$0, 7^1, (6^1), (7^15^1)$	$0, 7^1, (6^1), (7^15^1)$
8^17^2	8^17^1	$0, 8^17^1, 8^1, 7^15^1$	$0, 8^17^1$
8^15^1	$0, 5^1, 8^1$	$0, (5^16^1), 8^1$	$0, (5^16^1)$
2^1	$0, 7^1$ + other unassigned	$0, 7^1$ + other unassigned	0

The bracketed SVL's in Columns B and C indicate final levels energetically inaccessible in the case of complex dissociation.

occurs for collisions while it is absent in the van der Waals complex dissociation.

A qualitative interpretation of the observations cited, which is consistent with the interpretation of the very low energy collision induced relaxation of I_2, can be constructed as follows. We first note that over the entire range of effective collision energies the de Broglie wavelength of the He atom is never less than a typical internuclear spacing of the polyatomic molecule. Indeed, in the case of the lowest energy collisions the He de Broglie wavelength is of the order of the size of the molecule. We now suggest that the scattering resonances associated with different vibrational levels have different energies, ordered with respect to the number of nodes of the vibrational level.[4] A correlation of this type is consistent with a collision configuration in which the slowly moving He atom "envelopes" a polyatomic collision partner which supports vibrational motion that is very rapid relative to the He atom motion. Then, because of the short range repulsion between the He and the bound atoms of the molecule, we must expect the molecular vibration to force motion in the delocalized He distribution with the same symmetry as the vibration. The existence of this forced motion has two consequences. First, the He delocalized wavefunction will have nodes which correspond to the nodes of the vibrational mode, which leads to an increase in the energy of the scattering resonance when the number of nodes increases. Second, the driven motion of the He atom distribution generates a reaction force with the correct frequency and symmetry to affect rapid depopulation of the driving mode. For example, mode l^1 of $^2B_2$ aniline is a breathing motion of the aromatic ring, so it is capable of supporting a nodeless scattering resonance with He, whereas mode 13^1 has six nodes in the carbon skeleton motion. Our interpretation suggests that because of this difference in nodal patterns, the scattering resonance supported by l^1 will lie lower than that supported by 13^1, with corresponding cessation of effective collision induced depopulation at smaller $\hat{x}$ for 13^1 than for l^1, as is observed.

The one case we have found for which very low energy collision induced vibrational relaxation is not extraordinarily efficient is benzene.[5] Given that both benzene and I_2 are nonpolar (whereas all other species studied have a nonzero dipole moment), this is a very puzzling inconsistency. Perhaps the inefficiency of the very low energy

process for benzene arises from the nature of the repulsive interaction between the scattering atom and the polyatomic molecule. In the case of I_2 the overall interaction, except for anisotropy, is not badly represented by a simple Lennard-Jones potential, but in the case of benzene the center of attraction is displaced from the centers of repulsion, so the effective atom–molecule repulsion is a much steeper function of separation of centers of mass than for a Lennard-Jones potential. The consequence of this difference in repulsive terms is to modify the potential well shape and, plausibly, to destabilize a scattering resonance as one goes from I_2 to benzene.

There are a few features of the very low energy collision process, revealed by the He and H_2-^1A_u glyoxal experiments, which we have not yet mentioned. First, there can be competition between collision induced intersystem crossing and collision induced vibrational relaxation, with the relative importance of the two processes apparently dependent on vibrational level, but not dependent on rotational level. Thus, Jouvet and Soep[15] find that very low energy collisions between He and ^1A_u glyoxal induce intersystem crossing with cross section 20–30 fold larger than the room temperature cross section for the same process. This observation is consistent with the scattering resonance mechanism described above. Second, when there are near degeneracies in the vibrational manifold, single collision multiple quantum transitions appear to make an important contribution to the relaxation pathway. Jouvet, Sulkes and Rice[6] find, for the case of very low energy collisions of He and ^1A_u glyoxal, many quantum relaxation to a variety of final levels involve the transitions $8^1 \rightarrow 6^1$ or $8^1 \rightarrow 7^1 5^1$ (see Figure 13). Now, 8^1 and 6^1 are nearly degenerate ($\Delta E = 17\ \text{cm}^{-1}$) as are 8^1 and $7^1 5^1$ ($\Delta E = 7\ \text{cm}^{-1}$). In the isolated molecule the symmetries of modes 8 and 6 are such that both Fermi resonance and Coriolis interaction are impossible. But, given the near degeneracy, it is possible that the removal of symmetry characteristic of the scattering resonance configuration, or of a collision, permits a small amount of mode mixing. If such mixing does occur during a collision, the apparently exceptional multiple quantum transition $8^1 \rightarrow 7^1 (\Delta E = 502\ \text{cm}^{-1})$ can be thought of as the sequence $8^1 \rightarrow 7^1 5^1$ via mixing in the scattering resonance, and $7^1 5^1 \rightarrow 7^1$ via dissociation of the scattering resonance. Finally, comparison of the energy distributions in the products of He-^1A_u glyoxal very low energy collisions and He-^1A_u glyoxal van der Waals molecule dissociation reveals that

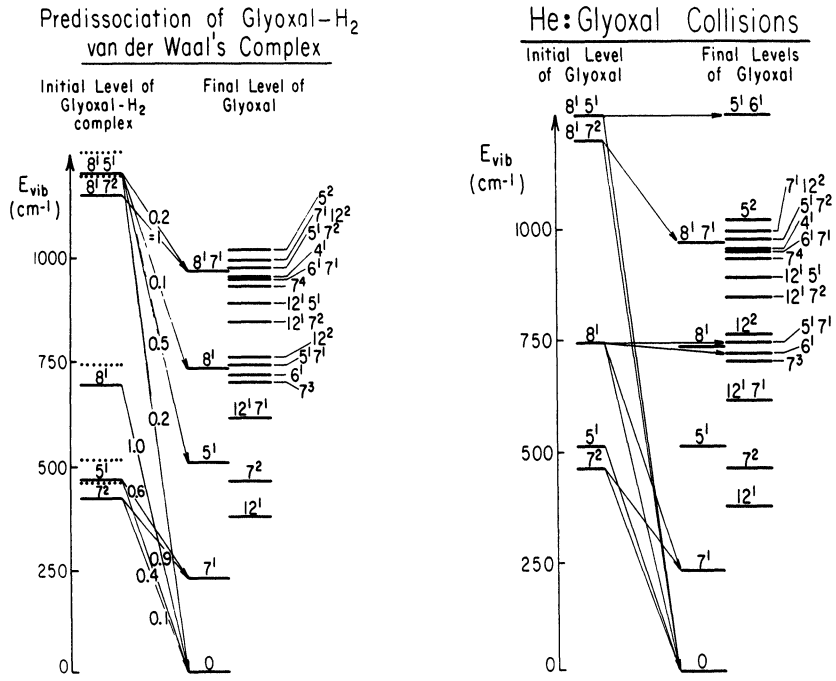

FIGURE 13 A comparison of the vibrational relaxation pathways characteristic of dissociation of the H_2 : glyoxal van der Waals complex and of very low energy He : glyoxal collisions. The former data are from ref. 8.

it is primarily the branching ratios to the final states that differ, with the identities of the final states for the two processes being sensibly the same.[7] This observation is consistent with the finding, by Halberstadt and Soep,[16] that for the 8^1 level of the H_2-glyoxal complex the branching ratio depends on the collision partner and on the feature of the complex excitation profile that is pumped.

4. RESULTS OF THEORETICAL STUDIES

As already mentioned in Section 1, understanding the observed anomalous enhancement of vibrational de-excitation at low collision energies provides an interesting theoretical challenge. All of the

simple theories of collision induced vibrational relaxation, such as that originally proposed by Landau and Teller[17] predict that the probability of vibrational relaxation becomes vanishingly small when the collision energy is very much less than the vibrational spacing. Theories using these ideas are qualitatively correct in the energy domain for which the de Broglie wavelength of the atom is very small relative to the internuclear spacings in the polyatomic molecule. For example, they adequately account for the falloff in rate of collision induced vibrational relaxation as the temperature of a gas falls. But the evidence discussed in Section 3 reveals that when the de Broglie wavelength of the atom is comparable to the internuclear spacings in the polyatomic molecule the cross section for vibrational relaxation is of the order of the geometric cross section.[3-7] Furthermore, the rapid decrease in scattering cross section with increasing energy for $E > 3\text{–}5\ \text{cm}^{-1}$ is not observed for rotational relaxation under the same conditions,[8] although the observed cross section is also very large.

To go beyond the qualitative analysis described in Section 3, and provide a proper theoretical basis for interpreting these results, Rice and coworkers have used several approaches. We shall describe these as follows: First, a formalism based upon an analogy with the analysis of neutron diffraction by molecules is proposed as a replacement for the exact close-coupling formalism of scattering theory.[10] Since atom–polyatomic molecule scattering is not amenable to a full quantum mechanical treatment, a qualitative means of understanding the experimental results is necessary. Even for smaller systems which might be studied by, say, the close-coupling formalism, a method based upon physically intuitive concepts will provide greater insight into the mechanism of scattering and energy transfer. Second, in the case of the simplest system studied experimentally, $He—I_2$, full three dimensional quantum mechanical scattering calculations have been performed within the close-coupling formalism.[9] These results yield the most accurate description of the scattering event possible. Third, a rotational infinite order sudden model is utilized to examine the $He—I_2$ rotational relaxation cross section.[18] This approximation, which is expected to be valid under the experimental conditions, provides support for the observed trends.[8]

It may seem that the theory of neutron diffraction can be immediately applied to describe very low energy atom–polyatomic molecule scattering, since the atomic wavefunction is primarily influenced by

the geometry of the molecule and does not modify the internal structure of the molecule. Unfortunately, this is not the case. In neutron scattering, the neutron-nucleus interaction is of such short range that each nucleus is a distinct and isolated scattering center with initial and final state neutron wave functions accurately described by plane waves. In atom–molecule scattering, the potential interaction is always strong enough to distort the wave function of the atom, invalidating the plane wave (Born) description. In order to retain the simplicity and physical content of the correlation function representation which describes neutron scattering, it is necessary to include the effects of the atom-molecule interaction, and the most direct method for doing so is to introduce the Distorted Wave Born Approximation (DWBA).

Cerjan, Lipkin and Rice have implemented the DWBA-correlation function representation of atom-polyatomic molecule scattering. The collision induced transition rate is, in terms of the T-matrix elements,

$$R = 2\pi \sum_{\alpha,\alpha'} p_\alpha |\langle \mathbf{k}'\alpha' | T | \mathbf{k}\alpha \rangle|^2 \delta(E - E' - \varepsilon) \tag{8}$$

where α and α' represent the exact initial and final eigenstates of the molecule, $\mathbf{k}$, and $\mathbf{k}'$, the corresponding momentum states of the projectile, and T is the full transition matrix. (Atomic units are used throughout.) The delta-function conserves energy in a process in which ε is the energy transferred to the atom as the molecular energy changes from E to E'. The probabilities, p_α, refer to the distribution of initial states. In the case where all the target molecules are prepared in a single state, α^*, as in a perfect jet experiment, p_α is the Kronecker delta $\delta_{\alpha\alpha^*}$.

Following Micha,[19] the rate expression (8) may be written as

$$\begin{aligned} R &= \sum_{\alpha,\alpha'} p_\alpha \int_{-\infty}^{\infty} dt\, e^{-i\varepsilon t} \langle \alpha | T^+_{\mathbf{k}'\mathbf{k}}(t) | \alpha' \rangle \langle \alpha' | T_{\mathbf{k}'\mathbf{k}} | \alpha \rangle \\ &= \sum_{\alpha,\alpha'} p_\alpha \int_{-\infty}^{\infty} dt\, e^{-i\varepsilon t} \langle \alpha | T^+_{\mathbf{k}'\mathbf{k}}(t) T_{\mathbf{k}'\mathbf{k}} | \alpha \rangle \end{aligned} \tag{9}$$

where use has been made of the Heisenberg representation and the completeness of the final states. To use the DWBA, the potential describing the atom–polyatom interaction is written as the sum of

two terms,

$$V = V_{\mathrm{I}} + V_{\mathrm{II}} \tag{10}$$

where the influence of V_{II} is presumed small relative to that of V_{I}. It is usual to choose the separation (10) so that one can solve the scattering problem excatly for V_{I}, generating a form for the scattered wave functions. Then corrections are obtained as a power series in V_{II}.

Let the total wavefunction be written as

$$\Psi_{\mathbf{k}\alpha} = \psi_\alpha \chi_{\mathbf{k}}(V) \tag{11}$$

where $\chi_{\mathbf{k}}$ is the exact atom wave function and we have explicitly indicated the dependence on V. It is then fairly straightforward to show that

$$\begin{aligned} T_{\mathbf{k}'\mathbf{k}} &= \langle \chi_{\mathbf{k}'}^{(-)}(V) | V_{\mathrm{II}} | \chi_{\mathbf{k}}^{(+)}(V_{\mathrm{I}}) \rangle + \langle \chi_{\mathbf{k}'}^{(+)}(V_{\mathrm{I}}) | V_{\mathrm{I}} | \phi_{\mathbf{k}} \rangle \\ &\simeq \langle \chi_{\mathbf{k}'}^{(-)}(V_{\mathrm{I}}) | V_{\mathrm{II}} | \chi_{\mathbf{k}}^{(+)}(V_{\mathrm{I}}) \rangle + \langle \chi_{\mathbf{k}'}^{(+)}(V_{\mathrm{I}}) | V_{\mathrm{I}} | \phi_{\mathbf{k}} \rangle \end{aligned} \tag{12}$$

where in constructing (12) we have discarded all higher powers of V than the first. The plusses and minuses refer to incoming and outgoing waves, respectively.

Letting

$$T_{\mathbf{k}'\mathbf{k}}^{\mathrm{I}} = \langle \chi_{\mathbf{k}'}^{(+)}(V_{\mathrm{I}}) | V_{\mathrm{I}} | \phi_{\mathbf{k}} \rangle \tag{13a}$$

and

$$T_{\mathbf{k}'\mathbf{k}}^{\mathrm{II}} = \langle \chi_{\mathbf{k}'}^{(-)}(V_{\mathrm{I}}) | V_{\mathrm{II}} | \chi_{\mathbf{k}}^{(+)}(V_{\mathrm{II}}) \rangle, \tag{13b}$$

and substituting (12) in (9), we find

$$\begin{aligned} R &= \sum_\alpha p_\alpha \int_{-\infty}^{\infty} dt\, e^{-i\varepsilon t} \langle \alpha | \{ (T_{\mathbf{k}'\mathbf{k}}^{\mathrm{I}})^+(t) + (T_{\mathbf{k}'\mathbf{k}}^{\mathrm{II}})^+(t) \} \{ T_{\mathbf{k}'\mathbf{k}}^{\mathrm{T}} + T_{\mathbf{k}'\mathbf{k}}^{\mathrm{II}} \} | \alpha \rangle \\ &= \int_{-\infty}^{\infty} dt\, e^{-i\varepsilon t} \{ \langle\langle (T_{\mathbf{k}'\mathbf{k}}^{\mathrm{I}})^+(t) T_{\mathbf{k}'\mathbf{k}}^{\mathrm{I}} \rangle\rangle + \langle\langle (T_{\mathbf{k}'\mathbf{k}}^{\mathrm{I}})^+(t) T_{\mathbf{k}'\mathbf{k}}^{\mathrm{II}} \rangle\rangle \\ &\quad + \langle\langle (T_{\mathbf{k}'\mathbf{k}}^{\mathrm{II}})^+(t) T_{\mathbf{k}'\mathbf{k}}^{\mathrm{I}} \rangle\rangle + \langle\langle (T_{\mathbf{k}'\mathbf{k}}^{\mathrm{II}})^+(t) T_{\mathbf{k}'\mathbf{k}}^{\mathrm{II}} \rangle\rangle \} \end{aligned} \tag{14}$$

with the standard notation for the expectation values inserted. This rate expression has been applied to systems which model the He—I_2 interaction[10,18] and, as expected, provides a substantial improvement over the cross section predicted by the Born approximation.

Further insight into the observed propensity rule for vibrational transitions[3] (see Section 3) can be obtained by writing the general T-matrix element as

$$T_{\mathbf{k}'\mathbf{k}}(\mathbf{R}) = \sum_j e^{if_j(\mathbf{R})} C_j(\mathbf{R}) \tag{15}$$

where f_j and C_j are real and include the possible anisotropic couplings. The rate expression is given by

$$R \sim \int_{-\infty}^{\infty} dt\, e^{-i\varepsilon t} \sum_{jj'} \langle\langle e^{-if_j(\mathbf{R}(t))} C_j(\mathbf{R}(t))\, e^{if_{j'}(\mathbf{R})} C_j(\mathbf{R}) \rangle\rangle \tag{16}$$

Expanding the time dependent terms in the rate expression to first order in the normal mode displacements of the molecule, and retaining only the downward transitions, the rate becomes

$$\begin{aligned} R \simeq & \sum_{jj'} \langle \alpha_{\text{vib}}^{(n)} | t_j^{(0)}(\mathbf{R}) t_{j'}^{(0)}(\mathbf{R}) | \alpha_{\text{vib}}^{(n)} \rangle \delta(\varepsilon) \\ & + \sum_{jj'} \sum_{\beta\beta'} a_\beta \langle \alpha_{\text{vib}}^{(n)} | t_{j\beta'}^{(1)} t_{j'}^{(0)}(\mathbf{R}) | \alpha_{\text{vib}}^{(n-1)} \rangle \delta(\varepsilon + \omega_\beta) \\ & + \cdots \end{aligned} \tag{17}$$

where $\alpha_{\text{vib}}^{(m)}$ denotes the mth vibrational state of the molecule and a_β is a constant depending upon the normal mode characteristics.

Several general features may be seen in the rate expression (17). First, the distorting effect of the potential, and possible multipolar couplings, are contained in the time independent elements. The magnitudes of these factors will significantly affect the possible scattering outcomes, controlling the amplitudes of the different potential contributions to the rate. Second, if each of the successively higher order processes decreases in magnitude, corresponding to an expected decrease in coupling as the separation of the states increases, then the vibrational transitions to nearest neighbor levels will generally be favored. For the weak interaction potentials assumed here, this assumption is probably valid, as manifested by the observed propensity rule for one vibrational quantum transfers. Third, if special symmetry restrictions constrain the internal motion of the system, then it is to be expected that certain vibrational energy transfer processes, which might otherwise be dominant, are not allowed or greatly suppressed.

It is also important to examine the low energy vibrational relaxation process as completely as possible from first principles. Due to the complexity of the quantum mechanical inelastic scattering problem, only the simplest system, He—I_2, can be adequately treated within the full close-coupling framework.[9]

The Schrödinger equation for the triatomic system He—I_2 is, for motion on one electronic surface,

$$\left[-\frac{1}{2\mu R^2}\frac{\partial}{\partial R}\left(R^2\frac{\partial}{\partial R}\right)+\frac{\mathbf{l}^2}{2\mu R^2}-\frac{1}{2mr^2}\frac{\partial}{\partial r}\left(r^2\frac{\partial}{\partial r}\right)+\frac{\mathbf{j}^2}{2mr^2}+V_{I_2}(r)+V_{\mathrm{He}-I_2}(R,r,\theta)\right]\psi^{JM}(\mathbf{R},\mathbf{r})=E\psi^{JM}(\boldsymbol{R},\boldsymbol{r}) \tag{18}$$

where $\mathbf{R}$ is the vector between the projectile He and the center of mass of the diatom I_2; $\mathbf{r}$ is the internal co-ordinate vector of the diatom; R and r are their associated magnitudes; θ is the angle between the vectors $\mathbf{R}$ and $\mathbf{r}$; m is the reduced mass of the diatom I_2 and μ is the He—I_2 reduced mass; $\mathbf{j}$ is the diatomic angular momentum operator and $\mathbf{l}$ is the He—I_2 angular momentum operator; $V_{I_2}(r)$ is the I_2 interaction potential and $V_{\mathrm{He}-I}(R, r, \theta)$ is the He–I_2 interaction potential.

Introducing a target state expansion and using the helicity body-fixed co-ordinate frame to simplify the interaction potential matrix element evaluations, the Schrödinger equation (18) may be integrated by a variety of techniques. These equations may be partially decoupled by the use of parity conservation which separates positive and negative total angular momentum projections, and by the homonuclear symmetry of the I_2, which separates even and odd rotational states.

After completion of the asymptotic analysis, the resulting T-matrix elements provide cross sections for the energetically allowed processes. The cross sections are given by the standard expression

$$\sigma(n'j'\leftarrow nj)=\frac{\pi}{2j+1}\frac{1}{k_j^2}\sum_{J=0}^{\infty}(2J+1)\sum_{ll'}|T^{(J)}_{n'j'l'\leftarrow njl}|^2 \tag{19}$$

where the $T^{(J)}_{n'j'l'\leftarrow njl}$ are the T-matrix elements for different (n, j, l) transitions with total angular momentum J and where $K_j^2=2\mu(E_{\mathrm{tot}}-E_{nj})$.

The potential chosen to represent the atom-molecule interaction is a pairwise sum of Morse functions, which is believed to be an accurate description for these systems[20]. The I_2 potential was deter-

mined by fitting spectroscopic data, and the He—I interaction was determined by examining the van der Waals pre-dissociation data for $He—I_2$.[21] With these choices, the integration of the partially decoupled equations was carried out by using both the log-derivative[22] and VIVS integration schemes[23]. The basis set and integration parameters were varied until convergence was achieved. The variation of the calculated cross section with respect to increasing translational energy is given for the processes $(24, j \leftarrow 25, 0)$, $(24, j \leftarrow 25, 2)$, $(0, j \leftarrow 1, 0)$ and $(0, j \leftarrow 1, 2)$ in Figures 14, 15, 16 and 17 respectively. For the $(24, j' \leftarrow 25, j)$ cross sections only zero total angular momentum was included in the total cross section sum, whereas $J = 0$, 1, 2, are included in the $(0, j' \leftarrow 1, j)$ results. These calculations show that the qualitative interpretation of the enhanced low energy vibrational relaxation cross section proposed by Rice and co-workers is correct: the cross section becomes vanishingly small for energies greater than a few cm^{-1}.

Finally, calculations of the rotational relaxation cross section were performed[18] using the same techniques as in the vibrational relaxation study. These calculations, though, are not exact since a rotational infinite order sudden approximation was used. That is, it was assumed that the basis set expansion for the entire wave function is restricted to one vibrational manifold. This approximation is suggested by a similar analysis of the vibrational pre-dissociation of $He—I_2$.[24] With this restricted basis set expansion, total cross sections (summed over all contributing total angular momentum J) could be obtained for three different sets of parameters for the pairwise atom–atom Morse functions:

a) $D = 7.0\ cm^{-1}$, $\beta = 1.24\ Å^{-1}$, $r_e = 4.0\ Å$
b) $D = 18.5\ cm^{-1}$, $\beta = 1.14\ Å^{-1}$, $r_e = 4.0\ Å$
c) $D = 17.5\ cm^{-1}$, $\beta = 1.20\ Å^{-1}$, $r_e = 4.6\ Å$

Figures 18 and 19 display the rotational de-excitation processes $(0, 0 \leftarrow 0, j)$ for the first two sets, while Figure 20 presents the $(25, 0 \leftarrow 25, j)$ processes for the third parameter set. For comparison, the uncorrected data of Tusa, Sülkes and Rice[8] are also included. (It should be noted that these data are for the $n = 28$ state rather than the $n = 25$ state.) Overall, it is clear that the calculations provide qualitative support for the experimental observations.

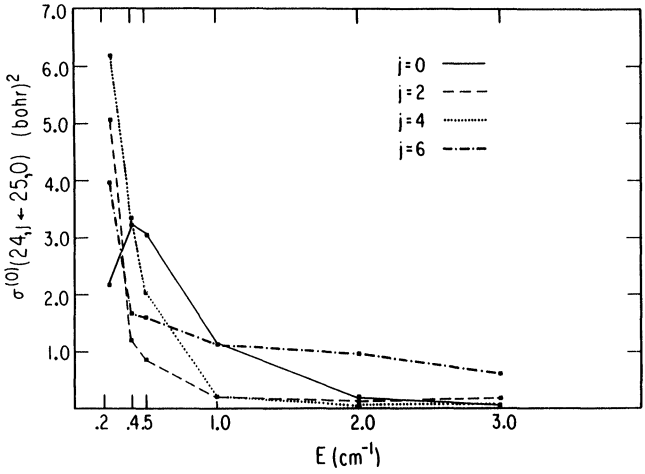

FIGURE 14 Energy variation of the zero total angular momentum cross section for vibrational de-excitation from ($n = 25, j = 0$) to ($n' = 24, j'$) for $j' = 0, 2, 4, 6$.

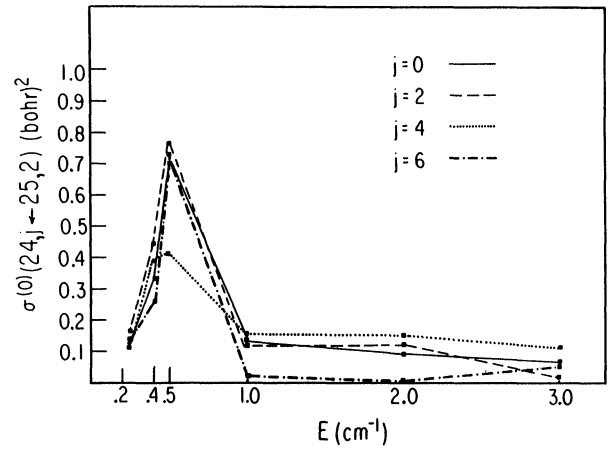

FIGURE 15 Energy variation of the zero total angular momentum cross section for vibrational de-excitation from ($n = 25, j = 2$) to ($n' = 24, j'$) for $j' = 0, 2, 4, 6$.

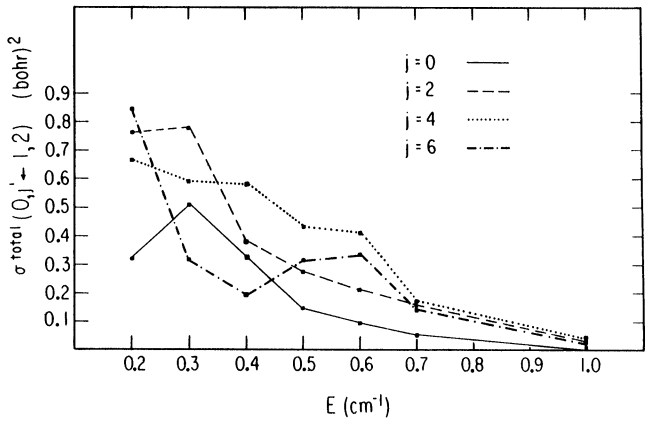

FIGURE 16 Energy variation of the cross section for the sum of the first three total angular momentum contributions, $\sigma^{\text{total}} = \sigma^{(0)} + \sigma^{(1)} + \sigma^{(2)}$, and vibrational de-excitation from $(n = 2, j = 0)$ to $(n' = 0, j')$ for $j' = 0, 2, 4, 6$.

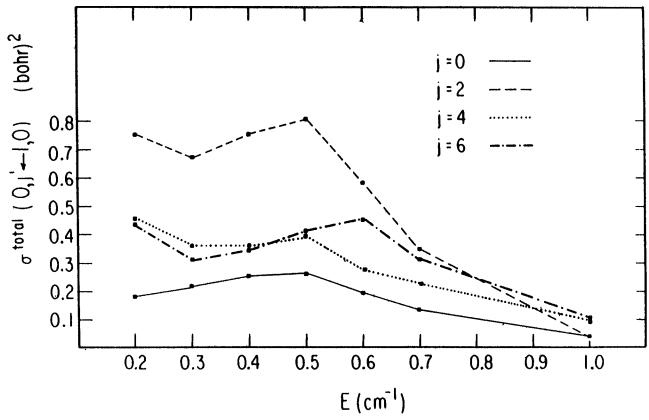

FIGURE 17 Energy variation of the cross section for the sum of the first three total angular momentum contributions, $\sigma^{\text{total}} = \sigma^{(0)} + \sigma^{(1)} + \sigma^{(2)}$, and vibrational de-excitation from $(n = 1, j = 2)$ to $(n' = 0, j')$ for $j' = 0, 2, 4, 6$.

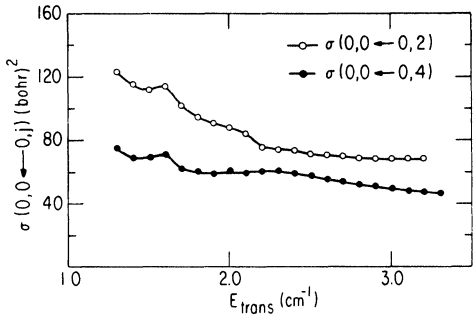

FIGURE 18 Energy dependence of the total cross section for two deexcitation processes in the $n = 0$ vibrational state, $\sigma(0, 0 \leftarrow 0, 2)$ and $\sigma(0, 0 \leftarrow 0, 4)$ using parameter set (a) of the text.

5. CONCLUDING COMMENTS

The very low energy collision induced relaxation of polyatomic molecules is rather different from the behavior predicted by models which do not fully incorporate the quantum dynamical features of the scattering process. The research reported in this paper, although showing a rather satisfying agreement between observation and theory, only scratches the surface—we are convinced that many more aspects of the very low energy process remain to be discovered, and that their interpretation will challenge the quality of our theoretical understanding of scattering phenomena.

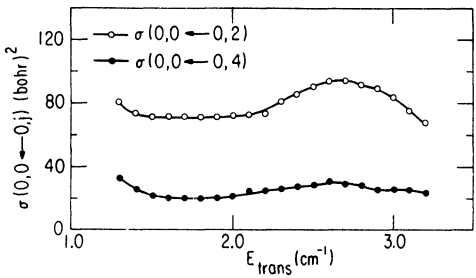

FIGURE 19 Energy dependence of the total cross section for two deexcitation processes in the $n = 0$ vibrational state, $\sigma(0, 0 \leftarrow 0, 2)$ and $\sigma(0, 0 \leftarrow 0, 4)$, using parameter set (b) of the text.

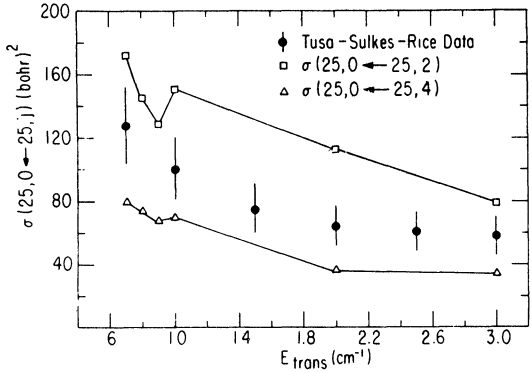

FIGURE 20 Energy dependence of the total cross section for two rotational de-excitation processes in the $n = 25$ vibrational state, $\sigma(25, 0 \leftarrow 25, 2)$ and $\sigma(25, 0 \leftarrow 25, 4)$ using parameter set (c) of the text. The Tusa–Sulkes–Rice uncorrected cross section is displayed for comparison.

Acknowledgements

This research has been supported by grants from the Air Force Office of Scientific Research and the National Science Foundation.

References

1. J. Tusa, M. Sulkes and S. A. Rice, *J. Chem. Phys.* **70,** 3136 (1979).
2. R. N. Schwartz, Z. I. Slawsky and K. Herzfeld, *J. Chem. Phys.* **20,** 1591 (1952).
3. M. Sulkes, J. Tusa and S. A. Rice, *J. Chem. Phys.* **72,** 5733 (1980).
4. J. Tusa, M. Sulkes, S. A. Rice and C. Jouvet, *J. Chem. Phys.* **76,** 3513 (1982).
5. C. Jouvet, M. Sulkes and S. A. Rice, *Chem. Phys. Lett.* **84,** 241 (1981).
6. C. Jouvet, M. Sulkes and S. A. Rice, *J. Chem. Phys.* in press.
7. M. Sulkes, C. Jouvet and S. A. Rice, *Chem. Phys. Lett.* in press.
8. J. Tusa, M. Sulkes and S. A. Rice, *Proc. Nat. Acad. Sci.* **77,** 2367 (1980).
9. C. Cerjan and S. A. Rice, *J. Chem. Phys.* in press.
10. C. Cerjan, M. Lipkin and S. A. Rice, *J. Chem. Phys.* in press.
11. J. P. Toennies, W. Wetz and G. Wolf, *J. Chem. Phys.* **71,** 614 (1979).
12. H. M. Liepmann and A. Roshko, *Elements of Gas Dynamics* (Wiley, New York, 1957).
13. R. Cattolica, F. Robben, L. Talbot and D. R. Willis, *Phys. Fluids* **17,** 1793 (1974).
14. J. A. Blazy, B. M. DeKoven, T. D. Russell and D. H. Levy, *J. Chem. Phys.* **72,** 2439 (1980).
15. C. Jouvet and B. Soep, *J. Chem. Phys.* **73,** 4127 (1980).
16. N. Halberstadt and B. Soep, *Chem. Phys. Lett.* **87,** 109 (1982).
17. L. Landau and E. Teller, *Phys. Zeit.* **10,** 34 (1936).
18. V. Sethuraman, C. Cerjan and S. A. Rice, submitted to *J. Chem. Phys.*
19. D. A. Micha, *J. Chem. Phys.* **70,** 565 (1979); *J. Chem. Phys.* **70,** 3165, (1979).

20. J. A. Beswick and J. Jortner, in: *Advances in Chemical Physics*, XLVII, Part I, eds. J. Jortner, R. Levine and S. A. Rice (Wiley, New York, 1981) p. 363.
21. D. H. Levy, in: *Advances in Chemical Physics XLVII*, Part I, eds. J. Jortner, R. Levine and S. A. Rice (Wiley, New York, 1981) p. 323.
22. B. R. Johnson, *J. Chem. Phys.* **67,** 4086 (1977); **69,** 4678 (1978).
23. G. A. Parker, T. G. Schmalz and J. C. Light, *J. Chem. Phys.* **73,** 1757 (1980).
24. J. A. Beswick and G. Delgado-Barrio, *J. Chem. Phys.* **73,** 3653 (1980).